JOURNAL OF THE BALKAN GEOPHYSICAL SOCIETY, Vol. 2, No 2, May 1999, p. 30-45, 10 figs.

An algorithm for the 3-D inversion of tomographic resistivity and induced polarisation data: Preliminary results

P.I. Tsourlos [*] and R.D. Ogilvy [**]

[*] GeoMentor e.e.i.g., Sarantaporou 8, 15342 Agia Paraskevi, Athens, Greece
[**] British Geological Survey, Keyworth, Nottingham NG12 5GG, UK

(Received 15 January 1998; accepted 25 August 1998)

Abstract: *An algorithm for the 3-D inversion of dc-resistivity and induced polarisation cross-borehole data is presented. The procedure is fully automated and is based on a 3-D finite element forward modelling algorithm. The inversion is achieved by a smoothness-constrained algorithm and uses sophisticated data error treatment. The features of the algorithm are presented in detail. Tests of the algorithm with synthetic data are presented as well. The preliminary results indicate that the algorithm is robust, noise insensitive and it produces good quality inversions. Further testing of the algorithm with real data is necessary in order to prove its full potential.*

Key Words: *3D Resistivity, IP Inversion*

INTRODUCTION

Electrical resistivity and induced polarisation tomography techniques are increasingly used for a wide range of environmental and engineering geophysics problems.

The use of tomographic imaging is of considerable current interest due to the development of the technology associated with automatically multiplexed borehole electrode arrangements and automatic measuring systems which facilitate the acquisition of a large number of measurements in a limited time. However, it is essential to develop reliable and robust interpretation-inversion algorithms, which are able to produce a “deblurred” subsurface image in order to render the information accessible to non-experts. Further, since most of the problems associated with environmental and engineering geophysics are of a three-dimensional nature it is essential that these algorithms are developed for three-dimensions.

The traditional methods of graphical data interpretation, such as the construction of a pseudosection (Edwards, 1977) or an operator-controlled data fitting technique (e.g. Stretenovic and Marcetic, 1992) cannot be used to interpret tomographic resistivity data. Approximate such as the back-projection technique (Shima, 1991; Noel and Walker, 1991) can produce artefacts and their results are still not easily accessible to non-experts.

The advent of fast computers has allowed the development of resistivity and IP inversion schemes that provide an estimate of the subsurface resistivity and polarizability distribution consistent with the experimental data. This is a fully non-linear procedure and its "accurate" treatment involves iterative full-matrix inversion algorithms that can give good quality results. The inversion of earth resistivity and IP data is an ill-conditioned problem. Large variations in physically defined parameters may result into small variations in the observed data that make the inversion algorithm unstable. Additionally, factors such as the noise contamination of the data and an unsuccessful choice of the parameterised blocks can further increase this instability. In tomographic data sets involving the measurement of numerous electrode combinations, low data quality and measurements of low sensitivity can become an increasingly serious problem.

Several non-linear resistivity and IP inversion algorithms which can handle ill-conditioning have been reported in the literature mainly based on the damped least-squares algorithm also known as the Levenberg-Marquadt method (Trip *et al*., 1984; Smith and Vozof, 1984; Pelton *et al*., 1978). The Levenberg-Marquadt method can produce very good results but spurious noise-related artefacts can appear in the case of noisy data. Further, the produced results will be highly dependent on the "accidental" (successful or

not) choice of the initial model (Constable *et al*., 1987).

One other way to tackle the instability of the inverse problem is to impose a smoothness constraint. This technique has been proposed for the geophysical case by Constable *et al*. (1987) who named it Occam inversion (due to the 14th century philosopher) and he applied it to the 1-D resistivity and magnetotelluric inverse problems. The smoothness constraint inversion will produce a simplified model which is a reasonable representation of the subsurface and at the same time guarantees the inversion stability and most importantly produces a model which is based on the characteristic that the user has chosen (namely the pattern of the smoothness) and not on some arbitrary initial guess. Smoothness constrained algorithms for the surface earth resistivity case have been presented by Sasaki (1989), Xu (1993), Elis and Oldenburg (1994), Tsourlos (1995), Loke and Barker, (1996). Further, Oldenburg and Li (1994) presented schemes that imposed a smoothness constraint in the inversion of IP data.

Inversion schemes of cross-borehole tomographic data-sets has been reported by LaBreque and Ward (1990) who used Marquadt's method for inverting cross-hole resistivity data. Sasaki (1994) presented a 3-D smoothness constrained algorithm for tomographic data inversion. In his tests he illustrated that the resolving ability of the cross-borehole resistivity arrays decreases into the centre of the reconstructed area away from the boreholes. LaBreque *et al.* (1996a,b,c) presented a reconstruction algorithm for two and three dimensions which uses a smoothness constrained algorithm which differentiates from the typical smoothness constrained inversion (Occam's) in the way the Lagrangian multiplier is chosen. Morelli and LaBreque (1996) presented an improved version of the previous algorithm that incorporates the least-absolute deviation method for variable error weighting into the inversion procedure.

Within the framework of this work we extended the 3-D inversion of cross-hole resistivity data to include the inversion of induced polarisation data as well. The presented algorithm is designed to be fully compatible with the field data measured by a special cross-hole resistivity/IP field system which is currently under development.

The algorithm is an iterative one and is based on a 3-D Finite Element Method (FEM) scheme that is used as the platform for the forward resistivity calculations. The adjoint equation approach (McGillivray and Oldenburg, 1990) was incorporated into the FEM scheme in order to calculate the Jacobian matrix **J** (the derivatives of the observations in respect of changes of the model's resistivity) when necessary.

3-D FORWARD MODELLING USING THE FEM

The forward modelling technique seeks to find a solution of the differential equation that governs the flow of the electrical current in the ground, a Poisson equation:

$$\nabla \cdot (-\sigma \nabla V) = \nabla \cdot J \qquad (1)$$

where *ó* is the conductivity, *V* the potential and *J* is the current density. The right-hand side term of equation (1) describes the current sources and can be replaced by a Dirac delta function and a point current I. Thus, equation (1) becomes:

$$\nabla \cdot (-\sigma \nabla V) = I\,\delta_{(x)}\delta_{(y)}\delta_{(z)} \quad . \qquad (2)$$

The basic concept of FEM is to subdivide the area into subregions (elements) in which the unknown potential *V'* is approximated by simple interpolator functions linked to specific points called nodes. For the hexahedral elements used here (eight nodes, at the vertices) a homogeneous and isotropic distribution of conductivity is assumed. The approximated potential (*V')* is given by:

$$V' = \sum_{i=1}^{8} n_i u_i \qquad (3)$$

where u_i is the nodal potential at the i^{th} node and n_i (i = 1,2,….8) are the so-called "shape functions" which for an hexahedral element are:

$$n_i = \frac{1}{8a^2b^2c^2}(a^2 + xx_i)(b^2 + yy_i)(c^2 + zz_i) \qquad i=1,2,\ldots,8 \qquad (4)$$

where the hexahedron is a brick with faces parallel to the co-ordinate axes, and dimensions 2a, 2b, 2c in the x,y,z directions, respectively.

Under the FEM considerations (homogeneous and isotropic earth within each element) the initial equation (2) for each individual element becomes:

$$-\sigma \nabla V^2 = f_{(x,y,z)} \qquad (5)$$

where $f_{(x,y,z)}$ is $I\,\delta_{(x)}\delta_{(y)}\delta_{(z)}$ or zero depending on whether current is inserted into the element or not.

An optimisation criterion should now be defined so that the difference between the approximated and the "real" potential becomes minimal. The most popular and general criterion in FEM analysis is the Galerkin weighted residual method, which states that the residual must be orthogonal to the basis functions

within each element.

Under the Galerkin minimisation technique the equation for the eth element becomes:

$$\iiint_e \sigma \nabla^2 V' n_i \; dxdydz - \iiint_e f_{(x,y,z)} n_i \; dxdydz = 0 \qquad i=1,2,\ldots,8 \qquad (6)$$

By substituting equation (3) into equation (6) and by performing integration by parts yields:

$$\sum_{j=1}^{8} \sigma_e \iiint_e \left[\left(\frac{\partial n_j}{\partial x}\frac{\partial n_i}{\partial x} + \frac{\partial n_j}{\partial y}\frac{\partial n_i}{\partial y} + \frac{\partial n_j}{\partial z}\frac{\partial n_i}{\partial z} \right) dxdydz \right] u_j - \iiint_e f_{(x,y,z)} n_i \; dxdydz = 0 \quad i=1,2,\ldots,8 \qquad (7)$$

The integrals of the first term of equation (7) can be calculated analytically (Pridmore, 1978):

$$\iiint_e \frac{\partial n_j}{\partial x}\frac{\partial n_i}{\partial x} dv_e = \frac{x_i x_j}{8a^3bc}\left(c^2b^2 + \frac{1}{3}c^2 y_i y_j + \frac{1}{3}b^2 z_i z_j + \frac{1}{9} y_i y_j z_i z_j \right) = B_i B_j$$

$$\iiint_e \frac{\partial n_j}{\partial y}\frac{\partial n_i}{\partial y} dv_e = \frac{y_i y_j}{8b^3ac}\left(a^2c^2 + \frac{1}{3}a^2 z_i z_j + \frac{1}{3}c^2 x_i x_j + \frac{1}{9} x_i x_j z_i z_j \right) = C_i C_j \qquad i,j = 1,2,\ldots,8 \qquad (8)$$

$$\iiint_e \frac{\partial n_j}{\partial z}\frac{\partial n_i}{\partial z} dv_e = \frac{z_i z_j}{8c^3ba}\left(a^2b^2 + \frac{1}{3}b^2 x_i x_j + \frac{1}{3}b^2 y_i y_j + \frac{1}{9} x_i x_j y_i y_j \right) = D_i D_j$$

The integrations are carried out over a hexahedral element ("brick") with x,y,z dimensions of 2a, 2b, 2c. Thus, the element equation can be written as:

$$\sigma_e \begin{bmatrix} B_1^2 + C_1^2 + D_1^2 & B_1B_2 + C_1C_2 + D_1D_2 & \cdots & B_1B_8 + C_1C_8 + D_1D_8 \\ & B_2^2 + C_2^2 + D_2^2 & \cdots & B_2B_8 + C_2C_8 + D_2D_8 \\ & \ddots & & \vdots \\ & & \ddots & \vdots \\ & \text{SYMMETRIC} & \ddots & \vdots \\ & & \ddots & \vdots \\ & & & B_8^2 + C_8^2 + D_8^2 \end{bmatrix} \begin{bmatrix} u_1 \\ u_2 \\ \vdots \\ \vdots \\ \vdots \\ \vdots \\ u_8 \end{bmatrix} = \begin{bmatrix} F_1 \\ F_2 \\ \vdots \\ \vdots \\ \vdots \\ \vdots \\ F_8 \end{bmatrix} \qquad (9)$$

The elements of the right hand side vector of equation (9) are zero when no current source coincides with an element's node or else becomes 2I.

Since elements will share common nodes the element equations can be assembled into a single set of linear equations. The resulting global system will have the general form

$$\mathbf{K} \,.\, \mathbf{U} = \mathbf{F} \qquad (10)$$

where the matrix **K** contains the stiffness terms (terms related to the nodal co-ordinates and element conductivities) and is square, sparse, symmetrical and banded, the vector **U** contains the nodal potential, and the matrix **F** contains the current sources and boundary terms.

After creation of this global system, the boundary conditions (BC) have to be considered: the Neumann BC (at the air-earth interface there is no current flow perpendicular to the boundary) are being enforced automatically via the element equation, while the homogeneous Dirichlet BC (the value of the potential at the side and bottom boundaries is zero) are enforced in the global system [equation 10]) in the form of constraint equations.

The final step is to solve the system of equations: for the 3-D case, which in general involves large systems of equations, an iterative technique is preferable. In this work, the conjugate gradient method for solving large sparse linear systems (Press *et al*., 1992) was used. As long as the system is solved and the nodal potential vector **U** is obtained, point to point potential differences and apparent resistivities are easily obtained. In Figure 1, a flow-chart of the 3D FEM algorithm is presented.

In order to illustrate the validity of the forward 3D FEM modelling scheme developed for this work, the

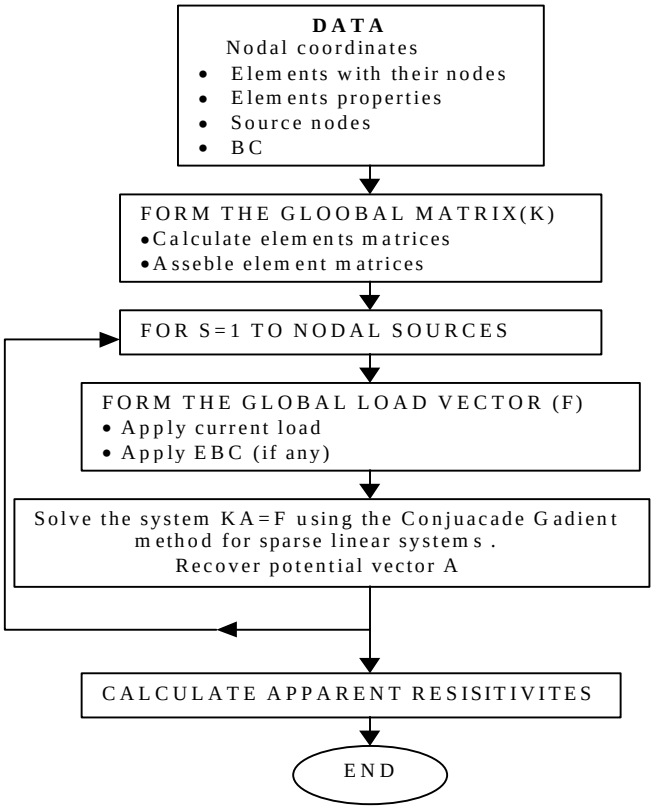

FIG 1. Flow chart of the 3-D FEM scheme used in this work.

results of the modelling of a dipole-dipole array over a prism are compared to the results obtained from the 3-D integral equation scheme (Pridmore, 1978) in Figure 2.

Modelling of the IP data

The modelling of the IP data is directly related to the modelling of the resistivity data. The IP effect can be described (Seigel, 1959) by a macroscopic physical parameter called chargeability *m* (a unit-less parameter confined to be in the region [0,1]). If **x** is the subsurface resistivity then the observed apparent resistivity vector **d** can be expressed as $\mathbf{d}=\boldsymbol{F}(\mathbf{x})$ where $\boldsymbol{F}$ is the forward modelling operator. The effect of the subsurface chargeability *m* can be expressed as

$$\mathbf{d_m} = \boldsymbol{F}\,[\mathbf{x} / (\mathbf{1}-\mathbf{m})\,].$$

The apparent chargeability vector $\mathbf{m}_a$ can be expressed as:

$$\mathbf{m}_a = \frac{(\mathbf{d}_m - \mathbf{d})}{\mathbf{d}_m} = \frac{(F[\mathbf{x}/(1-\mathbf{m})] - F(\mathbf{x}))}{F[\mathbf{x}/(1-\mathbf{m})]}, \qquad (11)$$

thus, in order to obtain the apparent chargeability we have to calculate the forward response twice with resistivities **x** and **x**(1-**m**), respectively. The IP response is then obtained using the equation (11). In Figure 3 the resistivity and IP response of a conductive prism is depicted.

THE INVERSION TECHNIQUE

During the 3-D resistivity/IP reconstruction procedure the subsurface is considered as a set of individual three-dimensional blocks (parameters) which are allowed to vary their resistivity independently. The aim is to calculate a subsurface resistivity estimate **x** for which the difference **dy** between the observed data $\mathbf{d}_{obs}$ and the modelled data $\mathbf{d}_{calc.}$ (calculated using the forward modelling technique) is minimised.

Since we are dealing with a non-linear problem this procedure has to be iterative. With every iteration an improved resistivity estimate is sought and eventually the procedure stops until certain convergence criteria are met (i.e. until the RMS error is practically stable). The Occam's inversion scheme was applied in order to produce a stable non-linear algorithm for the 3-D inversion of earth resistivity data. A general description of the algorithm follows.

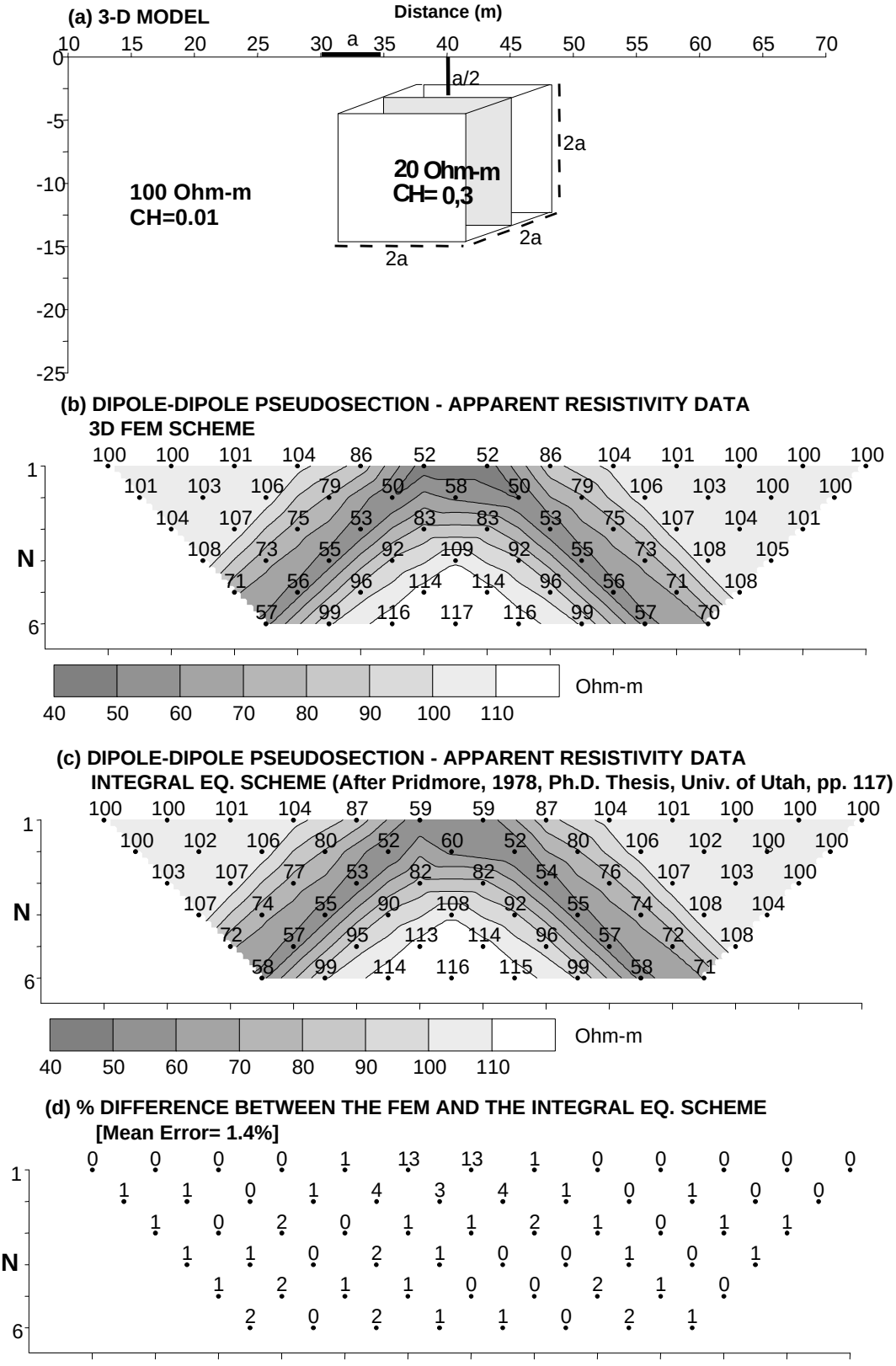

FIG. 2. Comparison of the dipole-dipole array results of the 3-D FEM scheme used in this work and the results obtained from the 3-D integral equation scheme (Pridmore, 1978).

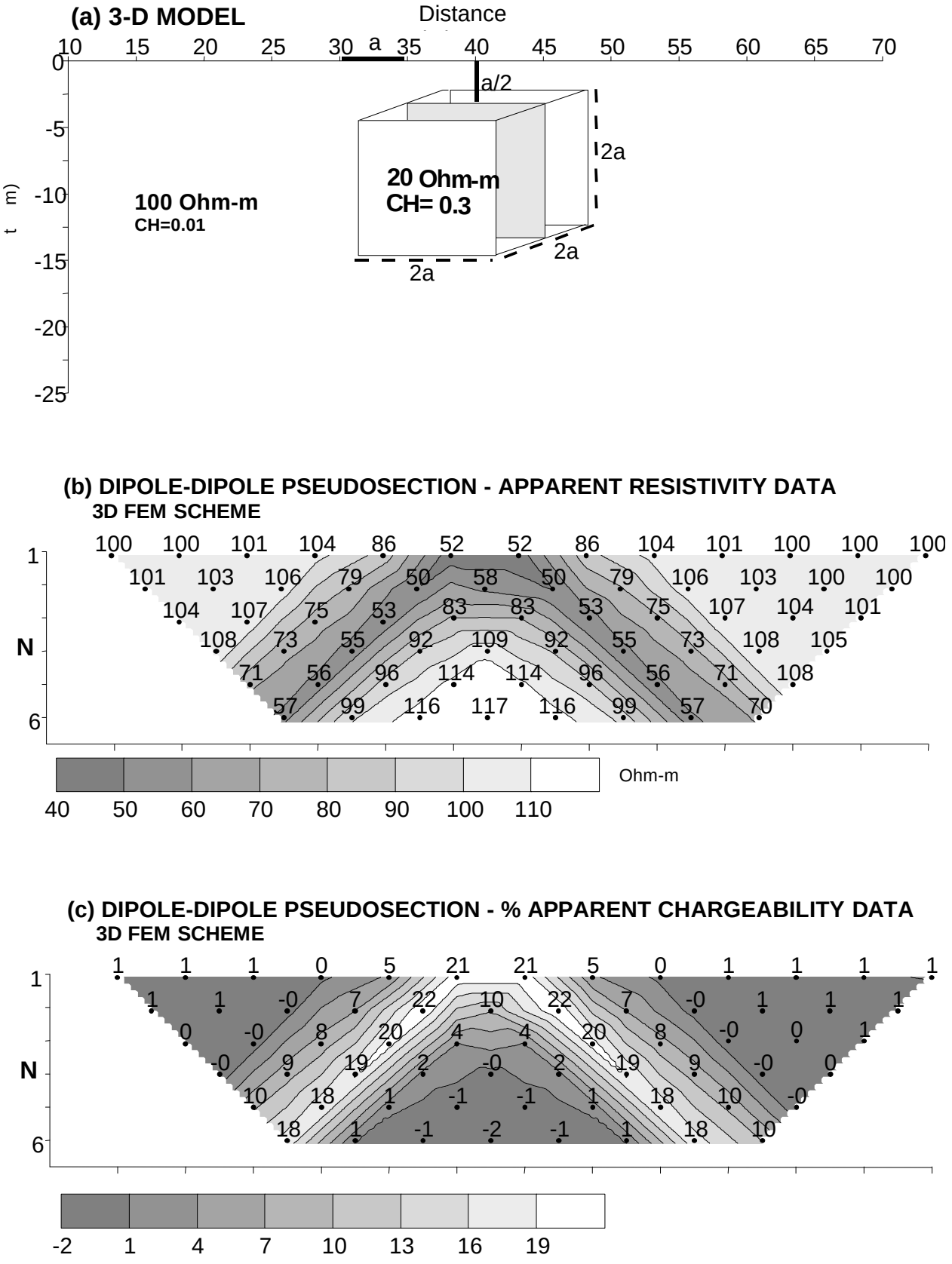

FIG. 3. The resistivity and IP response of a conductive prism (top) using the 3-D FEM scheme.

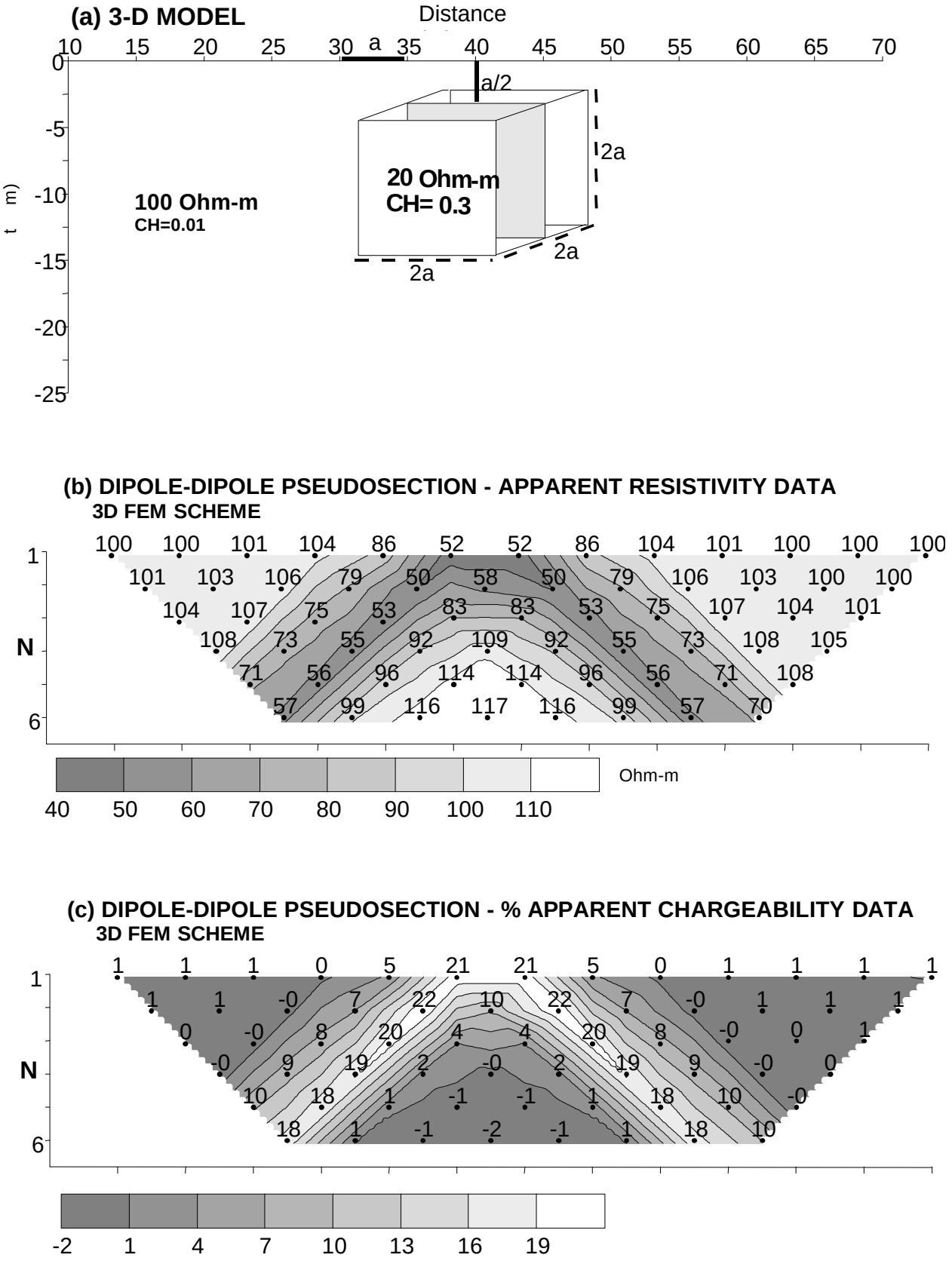

FIG. 3. The resistivity and IP response of a conductive prism (top) using the 3-D FEM scheme.

Initial Steps

Given a measured data set **y**

- Define the model parameters.
- Produce the matrix **C** that describes the smoothness pattern of the model.
- Define the error weighting matrix **W** which is a diagonal matrix ($\mathbf{W^T=W}$) which describes the accuracy of the measured data (includes the reciprocals of the data variances).
- Define an initial resistivity estimate $\mathbf{x_0}$ and calculate the model response $\mathbf{f(x_0)}$.
- Calculate the Jacobian matrix $\mathbf{J_0}$ that corresponds to $\mathbf{x_0}$.
- Set the initial value μ_0 of the Lagrangian multiplier.
- Set the inversion stopping criteria: slow convergence rate (practically stable RMS error) or divergence.

1. At the k^{th} iteration the resistivity correction vector $\mathbf{dx_k}$ is given by:

$$\mathbf{dx_k} = (\mathbf{W}\,\mathbf{J_k}^T\mathbf{W}\mathbf{J_k} + \mu_k\,\mathbf{C}^T\mathbf{C})^{-1}\,\mathbf{W}\mathbf{J_k}^T\mathbf{W}\mathbf{dy_k} \qquad (12)$$

where $\mathbf{J_k}$ is the Jacobian estimate which corresponds to the $\mathbf{x_k}$ resistivity distribution, and $\mathbf{dy_k} = \mathbf{y}-\mathbf{F}(\mathbf{x_k})$.

2. Set the new resistivity estimate $\mathbf{x_{k+1}}$ to $\mathbf{x_{k+1}} = \mathbf{x_k} + \mathbf{dx_k}$ and calculate the forward response of the new model $\mathbf{F}(\mathbf{x_{k+1}})$.

3. If one of the stopping criteria are met end the procedure else find the new estimate of the Jacobian matrix $\mathbf{J_{k+1}}$ and go to step 1.

Inversion of the IP data

The IP effect can be described by a macroscopic physical parameter called chargeability *m*. If **x** shows the intrinsic resistivities of the subsurface then the observed apparent resistivities can be expressed as $\mathbf{d}=\mathbf{F}(\mathbf{x})$ where **F** is the forward modelling operator. Similarly, the effect of the intrinsic chargeabilities can be expressed as $\mathbf{d_m}=\mathbf{F}[\mathbf{x}(1-\mathbf{m})]$. Consequently, the inversion of IP data can be related to the inversion of the resistivity data. See equation (11) that gives an expression for the apparent chargeability vector $\mathbf{m_a}$. Assuming that $\mathbf{F^{-1}}$ expresses the inverse operator the chargeability can be expressed as (Oldenburg and Li, 1994):

$$\mathbf{m} = (\mathbf{F}^{-1}[\mathbf{x}/(1-\mathbf{m})] - \mathbf{F}^{-1}(\mathbf{x})) / \mathbf{F}^{-1}[\mathbf{x}/(1-\mathbf{m})]. \qquad (13)$$

In other words the subsurface chargeability can be obtained by equation (13) after performing two inversions (using the described algorithm and identical inversion parameters) on the data sets obtained from the resistivity and the IP survey.

Inversion of Time-Domain Induced Polarisation (TD-IP) measurements

TD-IP measurements cannot be treated directly by the algorithm. TD-IP measuring systems usually record an integration of $V_{IP}(t)$ over a time window. Usually the measurement is expressed as:

$$P_{td} = (1/V_{DC}) \int_t V_{IP}(t)\,dt \ . \qquad (14)$$

This expression cannot be used directly as an input to the inversion program and it has to be converted into a form compatible with equations (11), (14). A way to do this is to recover a mean IP measurement V'_{IP} from each measured IP datum by using the formula:

$$V'_{IP} = V_{DC} \cdot P_{td} \cdot SF\ , \qquad (15)$$

where SF is a scaling factor which depends on the number of samples and the time window that was used. Subsequently, an expression of the apparent chargeability consistent with equation (13) can be obtained:

$$m_a = (V'_{IP} - V_{DC})/ V'_{IP} \qquad (16)$$

PRACTICAL CONSIDERATIONS

Some of the practical considerations of the algorithm are discussed below.

Variable error weighting

As long as the data errors are normally distributed and the data variances are accurately known then the scheme described in equation (12) will produce sufficiently accurate results. However, in many real cases, either the data variances are not accurately known or the error distribution is not normal. In tomographic measurements in particular, it is quite common that errors can be systematic due to poor electrode connections. For this reason the least-absolute deviations method, as described in LaBreque and Ward (1990) was incorporated into the algorithm. Broadly speaking, the technique increases the smoothness for those parameters that are recalculate the error-weighting matrix **W** in every iteration. The new i^{th} datum (W_{ii}) is expressed as:

$$_{new}W_{ii} = \begin{cases} {}_{old}W_{ii} & \text{if } {}_{trial}W_{ii} > {}_{old}W_{ii} \\ {}_{trial}W_{ii} & \text{if } {}_{trial}W_{ii} < {}_{old}W_{ii} \end{cases} \ . \qquad (17)$$

The trial datum is given by:

$$_{\text{trial}}W_{ii} = (W_{ii}^{1/2}/e_i)[\sum_j ({}_{\text{old}}W_{jj}^{1/2}e_j)/\sum_j ({}_{\text{old}}W_{jj}^{1/4}e_j^{1/2})]. \quad (18)$$

where e_i is the absolute value misfit of the i^{th} data point. The process of modifying the error-weighting matrix stops when it has no further effect over the L1 norm of the misfit error.

The parameterisation scheme

In order render the algorithm fully automated a scheme for automatic generation of the parameter space was included. In tomographic data the parameters are set as cubes with sides equal to the inter-electrode distance.

In our scheme, eight tetrahedral elements are assembled to create such a parameter (Figure 4 bottom). At the edges of the parameterised space more than eight elements are assembled to generate a parameter.

Further the option of assigning initial resistivities to each parameter layer was included. In many cases there is reliable prior information concerning the studied area (i.e. prior information from geoelectrical soundings about the layer structure in the studied area exists). Such information can be inserted into the program by assigning initial resistivities to the existing parameter layers in order to produce a parameterisation which is more consistent with the known geoelectrical structure of the area.

Smoothness matrix

The smoothness matrix **C** describes the smoothness relations between the parameters. The smoothness pattern in this algorithm is similar to the scheme proposed by Sasaki (1989, 1992). According to his scheme the roughness of the spatial variation of resistivity for a parameter j is given by:

$$d\mathbf{x}_j = a_j[dx_j^{\,k} + dx_j^{\,l} + dx_j^{\,m} + dx_j^{\,n} + dx_j^{\,o} + dx_j^{\,p} - 6dx_j] \quad (19)$$

where k,l,..p indicate the six immediate neighbours of the jth brick and a_j represents an empirically defined gradient-amplifying factor. If n is the number of parameters then C is a n x n matrix whose coefficients are a_j ,-6 a_j or 0. One possible choice for the factor a is to increase it gradually (i.e. a_j=1, 1.1,1.2 ...) as the distance of the parameter from the transmitting and receiving electrodes increases. Its value will reach the maximum at the central part of the reconstruction region. This reflects the decreasing resolution of the tomographic reconstruction in the central part of the image.

The Lagrangian Multiplier

In this scheme an empirical way for deciding the Lagrangian multiplier (LM) at every iteration is used. This scheme was preferred to the 1-D line search procedure (which tests several LM values and finds the optimum LM value by interpolation) since the later proved to be quite time-consuming: a modest line search needs at least three repetitions of the forward modelling and matrix inversion procedure.

The empirical scheme (which was established after several tests with synthetic and real data) is the following:

$$\mu_k = \mu_{k-1}/2 \quad \text{if } k \le 4$$
$$\mu_k = \mu_{k-1} \quad \text{if } k > 4 \quad . \quad (20)$$
$$k = 1,2,...,\text{number of iterations}$$

This scheme proved quite satisfactory and in the tested cases produced inversions very similar to those obtained by the 1-D line search scheme. Actually as Constable *et al*. (1987) suggested there is no guarantee that the 1-D line search procedure will produce a model that fits the data better. Thus, there is no reason to believe that the empirical scheme is inferior to the 1-D line search scheme.

EXAMPLES

The described algorithm was applied to a series of synthetic data. The finite element method was used as the forward modelling technique. The Jacobian matrix was calculated by the adjoint equation technique. The matrix inversion was performed by a conjugate gradient iterative technique that is able to cope with the increased computational needs of a 3-D scheme. A flow-chart of the described algorithm is presented in Figure 5.

Several tests were conducted in order to evaluate the performance of the algorithm. Two of them are presented here.

A pole-dipole cross-borehole data set (4 boreholes, 380 measurements) was obtained for the model of Figure 6: a resistive body with high polarizability within a two-layered earth. The data was contaminated with 7% random noise. In Figure 7 the results of the resistivity and IP inversion (13.500 elements, 5 iterations, 7.2% RMS) of the data obtained from the model of Figure 6 is presented as inverted parameter layers. In Figure 8 the three-dimensional inversion image of the subsurface polarizability of the same model is depicted.

A second pole-dipole cross-borehole data set (4 boreholes, 380 measurements) was obtained for the model of Figure 9. The data was contaminated with 7% random noise and the inverted resistivity and

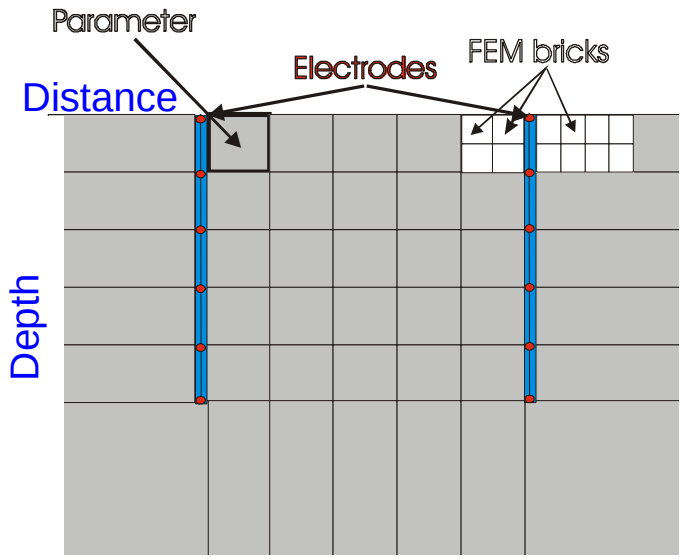

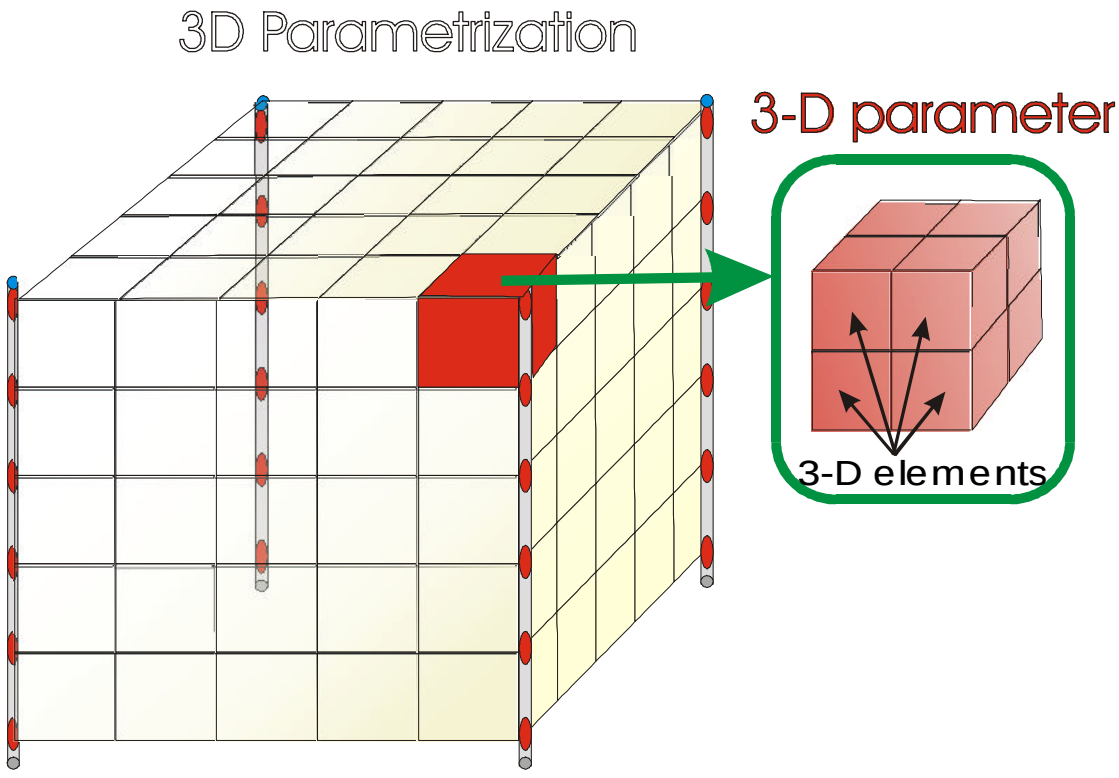

FIG. 4. Parameterisation for the case of 3-D cross-borehole data sets.

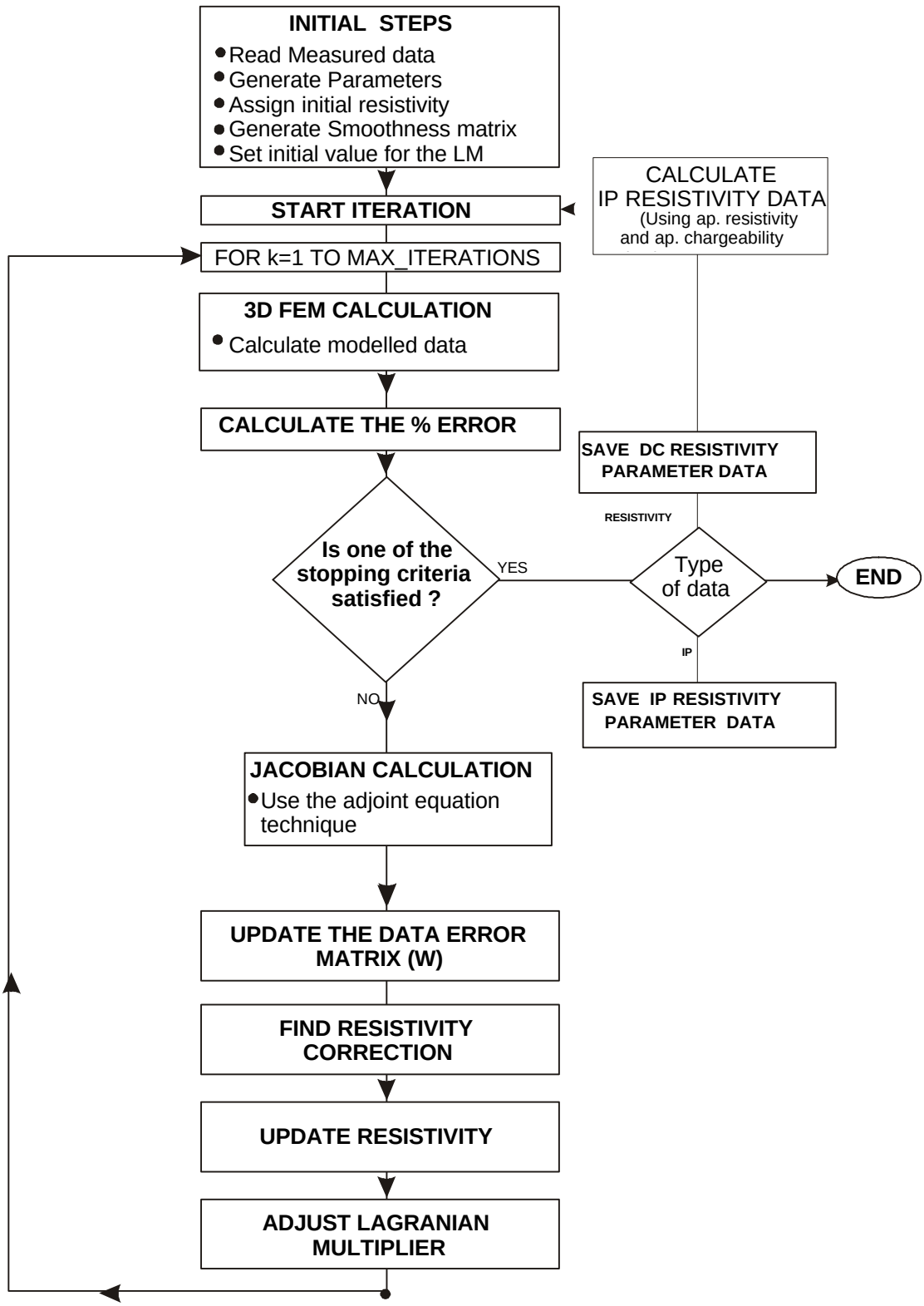

FIG. 5. Flow-chart of the 3-D resistivity / IP inversion algorithm.

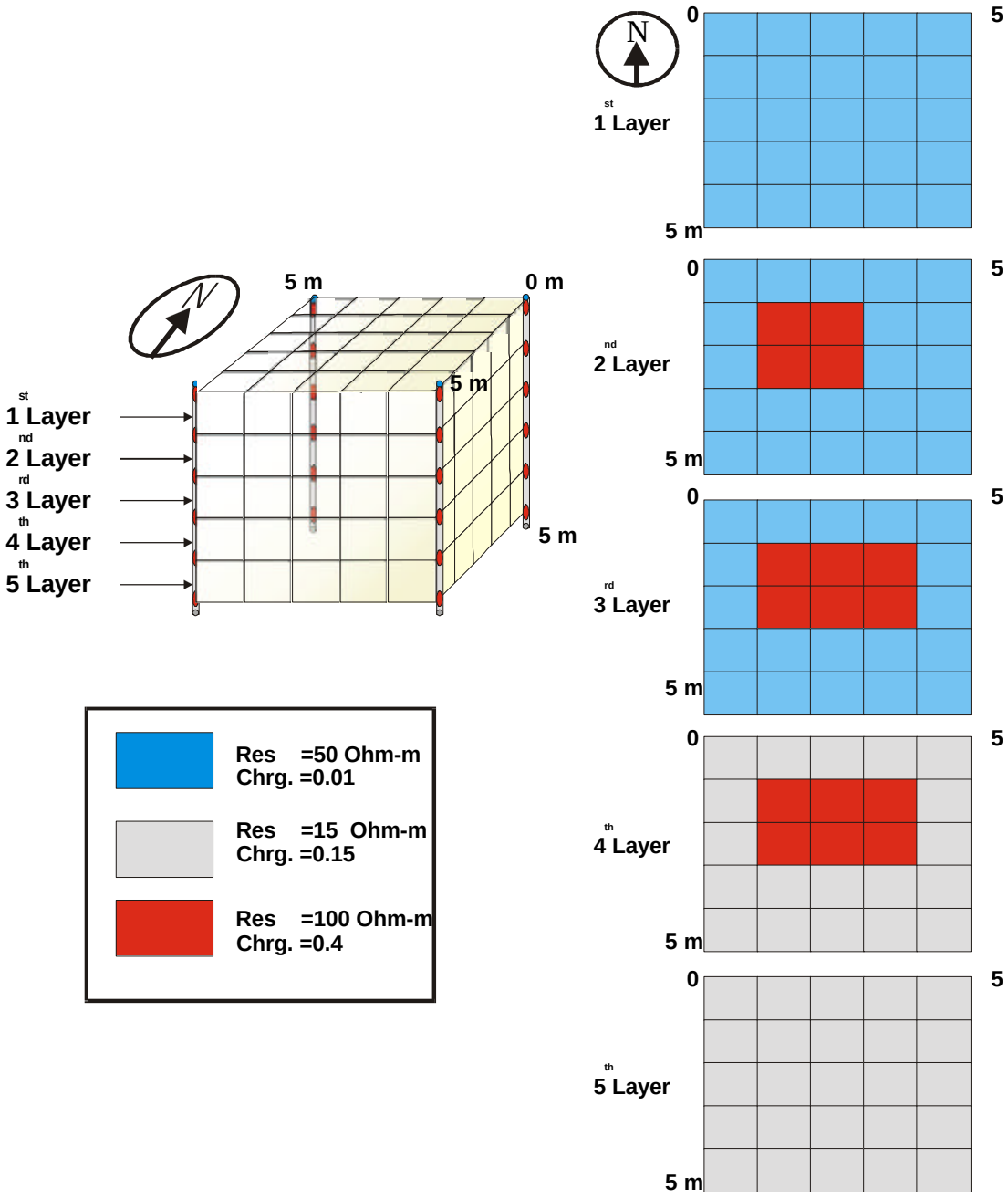

FIG. 6. The model used to produce a pole-dipole cross-borehole data set (4 boreholes, 380 measurements).

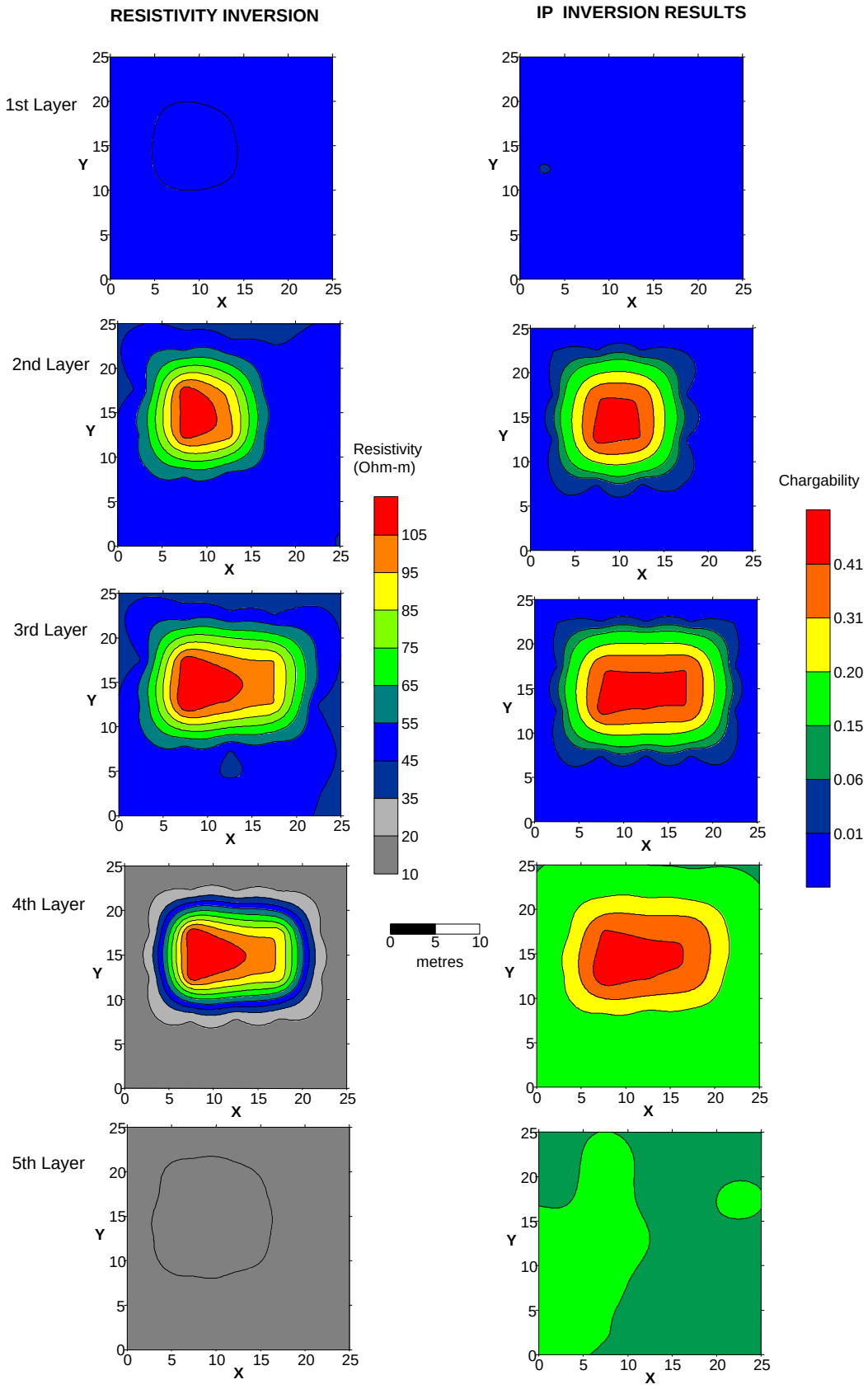

FIG. 7. 3-D inverted parameter layers (5 iterations, 7.2% RMS) of the resistivity and chargeability data (7% noise) obtained from the model of Figure 6.

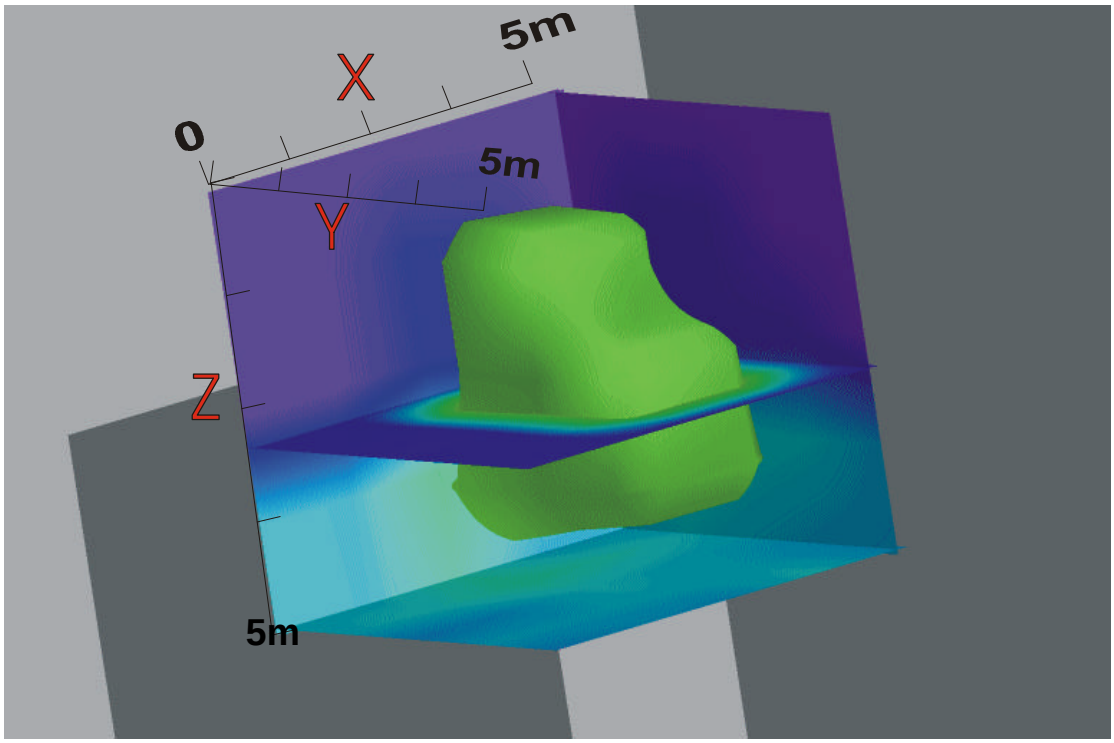

FIG. 8. 3-D inverted image obtained from the chargeability data for the model shown in Figure 6.

chargeability images (13.500 elements, 4 iterations, 7.4% RMS) of the cross-section of the central part of the area of interest are presented in Figure 10.

CONCLUSIONS

Within this work smoothness constrained algorithm for the inversion of tomographic resistivity and IP data was developed. The conducted tests with synthetic data indicated that:

- The algorithm comprises the advantages of stability, robustness to noise, inversion with user defined characteristics.
- Extra flexibility is achieved by allowing the incorporation of variable smoothness
- For all the tested cases with synthetic data the algorithm produced reasonably good results that do not suffer from algorithm and/or noise related artefacts.
- Overall, the algorithm is designed to address real field needs and to be reliable and useful for routine data interpretation. A further, extensive test with real data sets is required to prove the validity of the scheme and to fully investigate its potential.

REFERENCES

Constable, S. Parker, R., and Constable C., 1987. Occam's inversion: A practical algorithm for generating smooth models from electromagnetic sounding data: Geophysics, **52,** 289-300.

deGroot-Hedlin, C., and Constable, S., 1990.Occam's inversion to generate smooth, two-dimensional models from magneto-telluric data: Geophysics, **55**, 1613-1624.

Edwards, L.S., 1977. A Modified Pseudosection for Resistivity and IP: Geophysics, **42**, 1020-1036.

Ellis, R., and Oldenburg D.W., 1994. Applied geophysical inversion: Geophys.J.Int., 116, 5-11.

LaBrecque, D. and Ward, S., 1990. 2-D cross-borehole resistivity model fitting: In Ward, S (Ed.), Geotechnical and Environmental Geophysics, SEG, Tulsa, OK, 51-47.

LaBrecque, D., Miletto, M., Daily,W., Ramirez, A. and Owen, E., 1996a. The effects of noise on Occam's inversion of resistivity tomography data: Geophysics, **61**,538-548.

LaBrecque, D., Morelli, G., Undegrand, P., 1996b. 3-D electrical resistivity tomography for environmental monitoring: In Spies, B. (Ed), 3-D Electromagnetics, SEG, Tulsa, OK.

LaBrecque, D., Ramirez, A., Daily,W., Binley, M. and Schima, S., 1996c. ERT monitoring of environmental remediation process: Measurem. Sci. & Technol., **7**, 375-383.

Loke M.H. and Barker R., 1996. Rapid least-squares inversion of apparent resistivity pseudosections by a quasi-Newton method: Geophysical Prospecting, **44**, 131-152.

McGillivray, P., and Oldenburg, D., 1990. Methods for calculating Frechet derivatives and sensitivities for the Non-linear inverse problem: A comparative study: Geophysical Prospecting, **38**, 499-524.

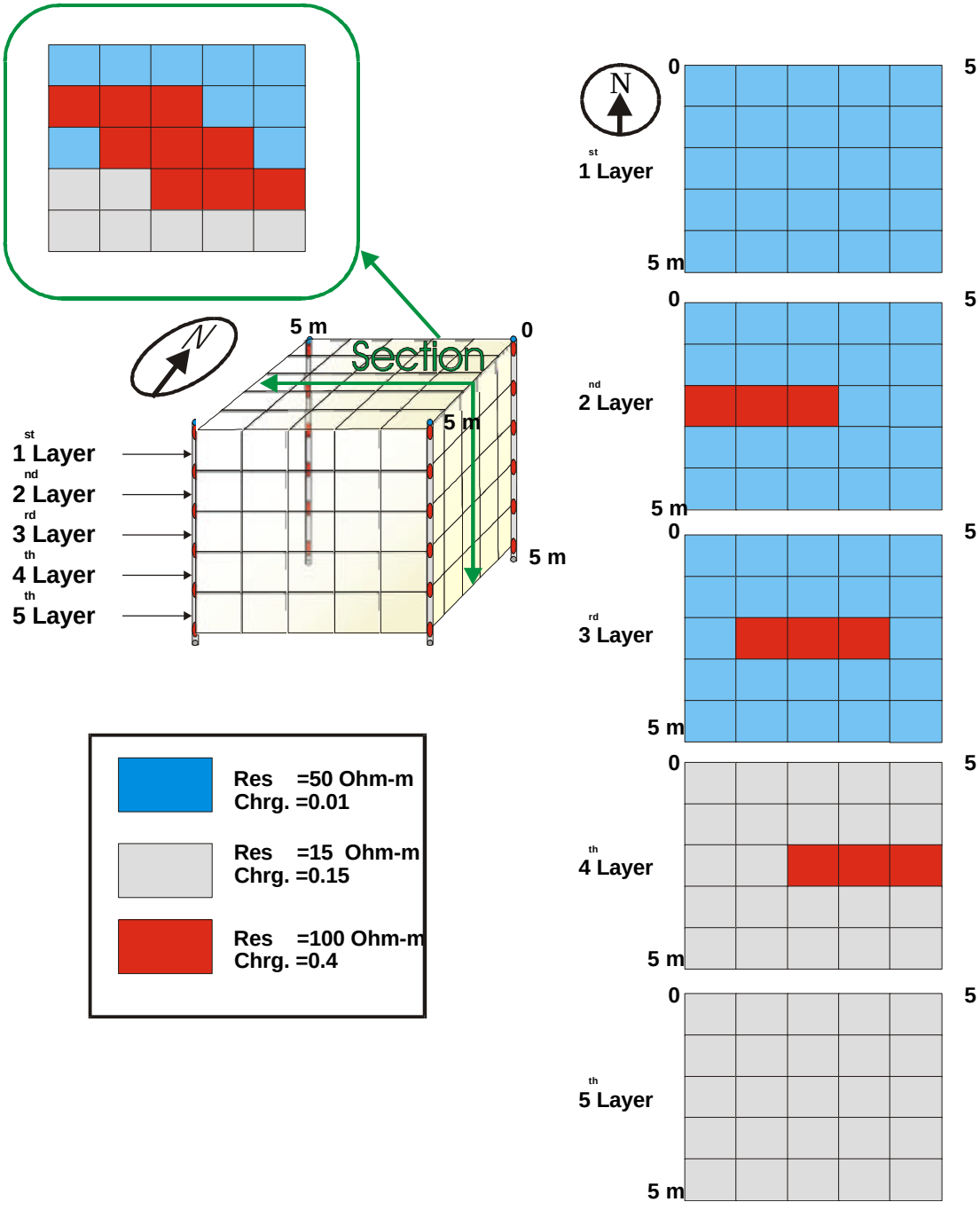

FIG. 9. The model used to produce a pole-dipole cross-borehole data set (4 boreholes, 380 measurements).

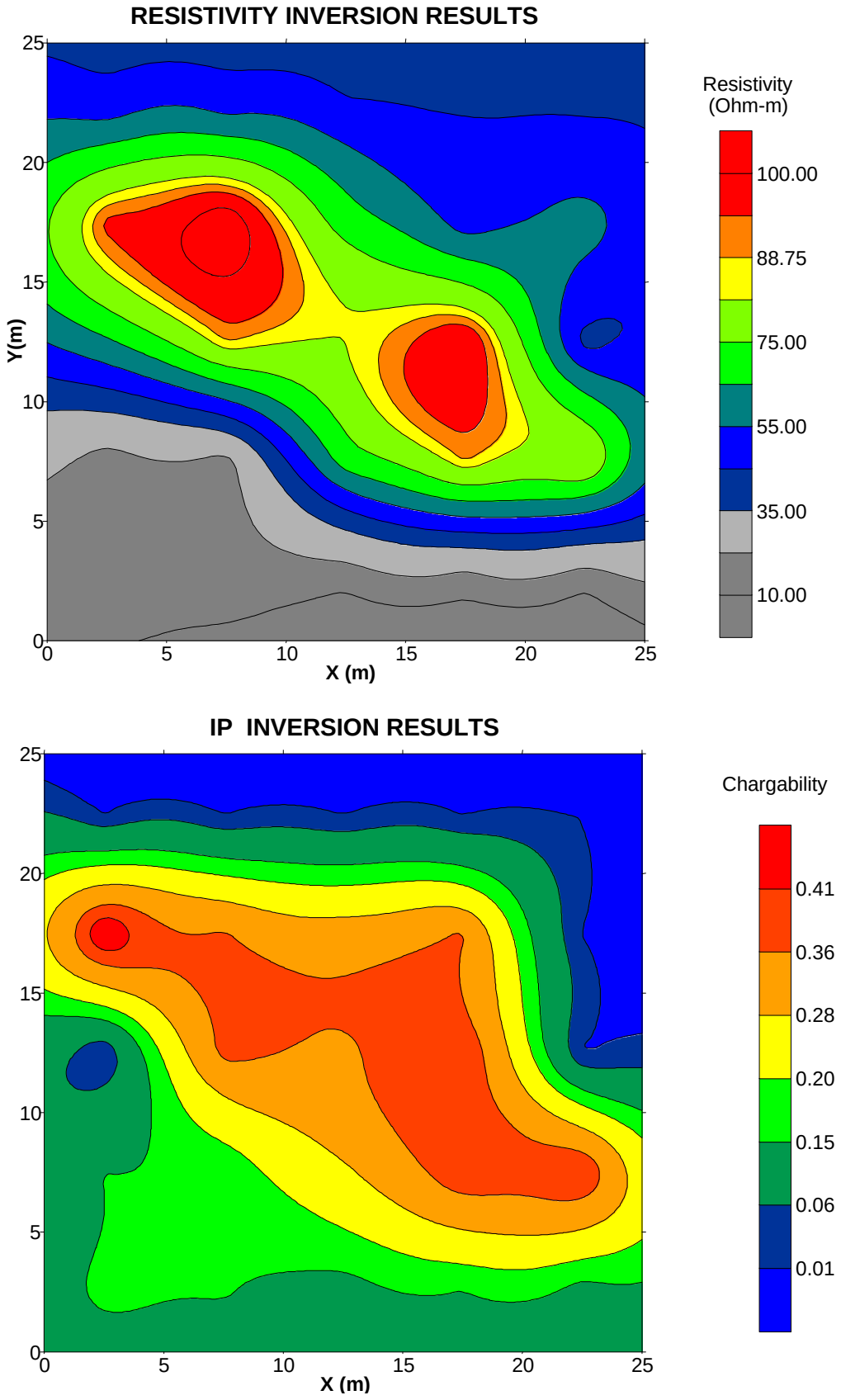

FIG. 10. 3-D inverted resistivity and chargeability sectional image of the central part of the parameterised space (4 iterations, 7.4% RMS) of the data (7% noise) obtained from the model of Figure 9.

Morelli, G. and LaBrecque, D., 1996. Advances in ERT inverse modelling: European Journal of Environmental and Engineering Geophysics, **1**,171-186.

Noel, M., and Walker R., 1991. Imaging archaeology by electrical resistivity tomography: a preliminary study: in Archaeological sciences 89, Budd, P., Chapman, B., Jackson, C. Janaway, R. and Ottaway, B., Oxbow, 295-304.

Oldenburg D. and Li Y., 1994. Inversion of induced polarisation data: Geophysics, **59**, 1327-1341.

Pelton, W., Rijo, L., and Swift, J., 1978. Inversion of two-dimensional resistivity and induced polarisation data: Geophysics, 43, 788-803.

Press, W., Flannery, B., Teukolski, S., and Vetterling, W., 1992. Numerical recipes, the art of scientific computing: Cambridge University Press.

Pridmore, D., 1978. Three-dimensional modelling of electric and electromagnetic data using the finite element method: Ph.D. Thesis, University of Utah.

Sasaki, Y., 1989. 2-D joint inversion of magnetotelluric and dipole-dipole resistivity data: Geophysics, **54**, 254-262.

Sasaki, Y., 1992. Resolution of resistivity tomography inferred from numerical simulation: Geophysical Prospecting, **40**, 453-464.

Sasaki, Y., 1994. 3-D resistivity inversion using the finite element method: Geophysics, **59**, 254-262.

Shima, H., 1991. Two-dimensional automatic resistivity inversion technique using alpha centres: Geophysics, 55, 682-694.

Siegel, H., 1959. Mathematical formulation and type curves for induced polarisation: Geophysics, **24**, 547-565.

Smith, N., and Vozoff, K., 1984. Two-dimensional DC resistivity inversion for dipole-dipole data: IEEE Trans. Geosc., **22**, 21-28

Stretenovic, B., and Marcetic, D., 1992. Determination of the internal geometry of a land-slide using electrical tomography: Abstracts of the 54th Meeting of the E.A.E.G., Paris, France, 1-5 June.

Tripp, A., Hohmann, G., and Swift, C., 1984. Two-dimensional resistivity inversion: Geophysics, 49, 1708-1717.

Tsourlos P., 1995. Modelling interpretation and inversion of multielectrode resistivity survey data: D. Phil. Thesis, University of York.

Xu, B., 1993. Development of electrical resistivity imaging methods for geological and archaeological prospecting: Ph.D. Thesis, University of Durham.